Articles

Tetragonal Zinc Diphosphide and Its Nanocomposite as an Anode for Lithium Secondary Batteries

Cheol-Min Park and Hun-Joon Sohn*

Department of Materials Science and Engineering, Research Center for Energy Conversion and Storage, Seoul National University, Seoul, 151-742, Korea

Received March 4, 2008. Revised Manuscript Received July 17, 2008

Tetragonal zinc diphosphide (ZnP_2) and its nanocomposite (ZnP_2/C) were prepared using commercially available amorphous red phosphorus and zinc powder by high energy mechanical milling (HEMM) at ambient temperature and pressure. The ZnP_2/C nanocomposite was composed of uniformly distributed, nanosized, ZnP_2 crystallites in the amorphous carbon matrix, as confirmed with X-ray diffraction (XRD) and high resolution transmission electron microscope (HRTEM) analyses. The electrochemical reaction mechanism of the ZnP_2/C nanocomposite with lithium was investigated during the first cycle. Electrochemical tests showed that the ZnP_2/C nanocomposite exhibited enhanced electrochemical reversibility, good cyclability, and high-rate capability when cycled between 0.55 and 2 V.

1. Introduction

Lithium ion rechargeable batteries are the most promising choice among rechargeable, solid-state batteries for mobile electronic devices and hybrid vehicles, due to their merits such as relative safety with a high energy density, good rate capability, and high power. Although graphite (372 mA h g^{-1})[1−3] is presently used as an anode material for lithium ion batteries, many higher-capacity alternatives are being actively pursued, of which Sn,[4−8] Si,[9−12] P,[13−18] Sb,[19−21] and Mg[22] based systems have attracted strong research attention due to their ability to react reversibly with large amounts of Li per formula unit. Although alloy-based systems have a higher energy density, they suffer from poor capacity retention, since a large volume change occurs during charge/discharge. Nowadays, nanostructured and nanocomposite electrode materials[23−26] for lithium-ion batteries have been studied intensively as an alternative electrode with high capacity, high rate capability, and stable cycling behavior, due to the ability of these materials to provide a higher interfacial area, increase the lithium ion diffusion rate, and accommodate the strain generated during cycling.

Since Souza et al. suggested the quasi-topotactic intercalation mechanism, in which lithium is inserted into the monoclinic binary MnP_4 phase to form the cubic ternary Li_7MnP_4 phase,[13] Li insertion/extraction in transition metal phosphides[15−18] has been investigated as a possible candidate for anode materials in lithium ion batteries. Recently, our group reported interesting results suggesting that black phosphorus and its composite are promising candidates as a

* Corresponding author. E-mail: hjsohn@snu.ac.kr.

(1) Dahn, J. R.; Zheng, T.; Liu, Y.; Xue, J. S. *Science* **1995**, *270*, 590.
(2) Winter, M.; Besenhard, J. O.; Spahr, M. E.; Novak, P. *Adv. Mater.* **1998**, *10*, 725.
(3) Yoshio, M.; Wang, H.; Fukuda, K. *Angew. Chem., Int. Ed.* **2003**, *42*, 4203.
(4) Idota, Y.; Kubota, T.; Matsufuji, A.; Maekawa, Y.; Miyasaka, T. *Science* **1997**, *276*, 1395.
(5) Lou, X. W.; Wang, Y.; Yuan, C.; Lee, J. Y.; Archer, L. A. *Adv. Mater.* **2006**, *18*, 2325.
(6) Park, M.-S.; Wang, G.-X.; Kang, Y.-M.; Wexler, D.; Dou, S.-X.; Liu, H.-K. *Angew. Chem., Int. Ed.* **2007**, *46*, 750.
(7) Zhang, Z.; Liu, Y.; Liu, M. *Chem. Mater.* **2006**, *18*, 4643.
(8) Noh, M.; Kim, Y.; Kim, M. G.; Lee, H.; Kim, H.; Kwon, Y.; Lee, Y.; Cho, J. *Chem. Mater.* **2005**, *17*, 3320.
(9) Yoshio, M.; Wang, H.; Fukuda, K.; Umeno, T.; Dimov, N.; Ogumi, Z. *J. Electrochem. Soc.* **2002**, *149*, A1598.
(10) Larcher, D.; Mudalige, C.; George, A. E.; Porter, V.; Gharghouri, M.; Dahn, J. R. *Solid State Ionics* **1999**, *122*, 71.
(11) Wen, Z. S.; Yang, J.; Wang, B. F.; Wang, K.; Liu, Y. *Electrochem. Commun.* **2003**, *5*, 165.
(12) Ng, S.-H.; Wang, J.; Wexler, D.; Konstantinov, K.; Guo, Z.-P.; Liu, H.-K. *Angew. Chem., Int. Ed.* **2006**, *45*, 6896.
(13) Souza, D. C. S.; Pralong, V.; Jacobson, A. J.; Nazar, L. F. *Science* **2002**, *296*, 2012.
(14) Park, C.-M.; Sohn, H.-J. *Adv. Mater.* **2007**, *19*, 2465.
(15) Kim, Y.-U.; Lee, C. K.; Sohn, H.-J.; Kang, T. *J. Electrochem. Soc.* **2004**, *151*, A933.
(16) Boyanov, S.; Bernardi, J.; Gillot, F.; Dupont, L.; Womes, M.; Tarascon, J.-M.; Monconduit, L.; Doublet, M.-L. *Chem. Mater.* **2006**, *18*, 3531.
(17) Woo, S.-G.; Jung, J.-H.; Kim, H.; Kim, M. G.; Lee, C. K.; Sohn, H.-J.; Cho, B. W. *J. Electrochem. Soc.* **2006**, *153*, A1979.
(18) Kim, Y.-U.; Cho, B. W.; Sohn, H.-J. *J. Electrochem. Soc.* **2005**, *152*, A1475.
(19) Park, C.-M.; Yoon, S.; Lee, S.-I.; Kim, J.-H.; Jung, J.-H.; Sohn, H.-J. *J. Electrochem. Soc.* **2007**, *154*, A917.
(20) Park, C.-M.; Sohn, H.-J. *Chem. Mater.* **2008**, *20*, 3169.
(21) Bryngelsson, H.; Eskhult, J.; Nyholm, L.; Herranen, M.; Alm, O.; Edstrom, K. *Chem. Mater.* **2007**, *19*, 1170.
(22) Park, C.-M.; Kim, Y.-U.; Kim, H.; Sohn, H.-J. *J. Power Sources* **2006**, *158*, 1451.
(23) Tarascon, J.-M.; Armand, M. *Nature* **2001**, *414*, 359.
(24) Arico, A. S.; Bruce, P.; Scrosati, B.; Tarascon, J.-M.; Schalkwijk, W. V. *Nat. Mater.* **2005**, *4*, 366.
(25) Derrien, G.; Hassoun, J.; Panero, S.; Scrosati, B. *Adv. Mater.* **2007**, *19*, 2336.
(26) Chan, C. K.; Peng, H.; Liu, G.; Mcilwrath, K.; Zhang, X. F.; Huggins, R. A.; Cui, Y. *Nat. Nanotechnol.* **2008**, *3*, 31.

10.1021/cm800632f CCC: $40.75
Published on Web 09/27/2008

new anode material for lithium secondary battery.[14] Black phosphorus has a layered structure consisting of puckered layers, and its composite showed good electrochemical performances when cycled between black P and LiP phase.

The Zn−P system has rich binary phases and polymorphisms, such as α-Zn_3P_2 (tetragonal), β-Zn_3P_2 (cubic), α-ZnP_2 (tetragonal), β-ZnP_2 (cubic), ZnP_2 (monoclinic), and ZnP_4 (monoclinic). Some research groups have recently reported Zn−P systems for Li batteries. Bichat et al.[27,28] and Kishore et al.[29] reported the electrochemical reactions of tetragonal Zn_3P_2 with Li, while Hwang et al.[30] reported the electrochemical reactions of monoclinic zinc diphosphide (ZnP_2) with Li. However, the reported results in these Zn−P binary systems for anode materials showed poor electrochemical behaviors. Among these binary phases, tetragonal ZnP_2 exhibits an interesting structure,[31] in which all the P atoms form singly bonded, infinite spiral chains, and the Zn atoms also form spirals approximately coaxial with the P chains.

In this report, we developed a simple method of transforming commercially available, amorphous red phosphorus and zinc powder into tetragonal ZnP_2 and its ZnP_2/C (Super P) nanocomposite using high energy mechanical milling (HEMM) at ambient temperature and pressure. Originally, tetragonal ZnP_2 was prepared at high pressure (0.5−2 GPa) and temperature (600−1000 °C).[32,33] It is well-known that the temperature during HEMM can rise above 200 °C and that the pressure generated can be of the order of 6 GPa,[34,35] conditions that are sufficient to transform red P and Zn into its alloying phase, that is, the tetragonal ZnP_2. In addition, the reaction mechanism with lithium and the electrochemical performances of tetragonal ZnP_2/C nanocomposite as an anode material for Li secondary batteries were investigated.

2. Experimental Section

Preparation of ZnP_2 and Its ZnP_2/C Nanocomposite. ZnP_2 was prepared with Zn (Kojundo, average size: 50 μm) and red P (Aldrich, average size: 100 μm) powders using HEMM (Vibratory mill, 700 rpm) at ambient temperature and pressure. Zn and P powders were put into a 80 cm^3 hardened steel vial with stainless steel balls (diameter: 3/8 in. and 3/16 in.) at a ball-to-powder ratio of 20:1. The HEMM process was conducted under an Ar atmosphere for 12 h. The same milling technique was employed for 12 h to produce the ZnP_2/C nanocomposite, as described above. Preliminary studies determined an optimum composition of ZnP_2 to carbon (Super P) of 70 to 30 by wt %. To identify impurities, such as iron, elemental analysis was conducted by EDS (energy dispersive spectroscopy) attached to SEM (scanning electron microscopy, JEOL, JSM-6360), and the results showed that only 0.07 wt % iron in the ZnP_2 powder and 0.09 wt % iron in the ZnP_2/C nanocomposite powder were detected, respectively.

(27) Bichat, M.-P.; Pascal, J.-L.; Gillot, F.; Favier, F. *Chem. Mater.* **2005**, *17*, 6761.
(28) Bichat, M.-P.; Monconduit, L.; Pascal, J.-L.; Favier, F. *Ionics* **2005**, *11*, 66.
(29) Satya Kishore, M. V. V. M.; Varadaraju, U. V. *J. Power Sources* **2005**, *144*, 204.
(30) Hwang, H.; Kim, M. G.; Kim, Y.; Martin, S. W.; Cho, J. *J. Mater. Chem.* **2007**, *17*, 3161.
(31) White, J. G. *Acta Crystallogr.* **1965**, *18*, 217.
(32) Stackelberg, M. V.; Paulus, R. *Z. Phys. Chem.* **1935**, *B28*, 427.
(33) Tanaka, Y. *The Review of Phys. Chem. of Japan* **1968**, *38*, No. 2.
(34) Suryanarayana, C. *Prog. Mater. Sci.* **2001**, *46*, 1.

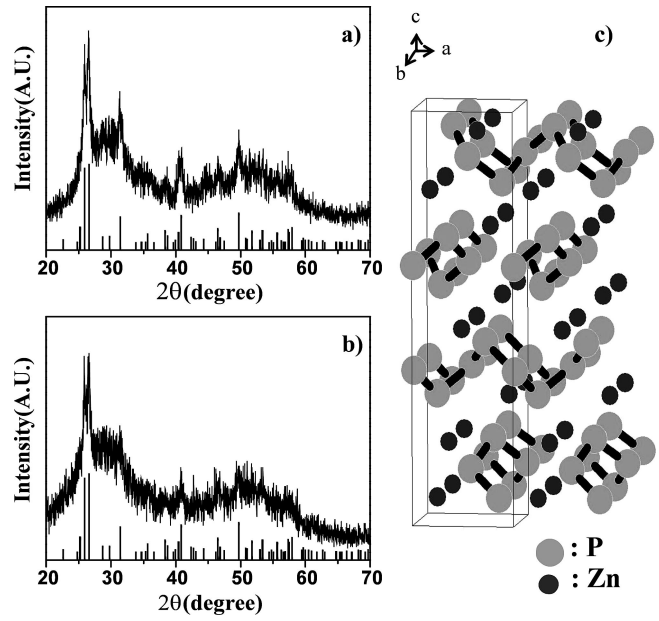

Figure 1. X-ray diffraction patterns and ball-stick models of crystal structure (JCPDS no. 72-1626): (a) ZnP_2, (b) ZnP_2/C nanocomposite, and (c) crystal structure of tetragonal ZnP_2.

Materials Characterization. ZnP_2 and ZnP_2/C nanocomposite samples were identified by X-ray diffraction (XRD, Rigaku, D-MAX2500-PC) and a high resolution transmission electron microscope (HRTEM, JEOL 3000F) operating at 300 kV. For the transmission electron microscope (TEM) observation, a dilute suspension of the sample was dropped on a carbon-coated TEM grid and dried. Ex situ XRD methods were used to observe the structural changes occurring in active materials during cycling. The electrodes were detached from the cell and coated by Kapton tape as a protective film to prevent any contamination from the air. Phases not observable by XRD pattern were analyzed by HRTEM.

Electrochemical Measurements. For the electrochemical evaluation of the ZnP_2 and ZnP_2/C nanocomposite samples, electrodes were prepared by coating slurries containing the active material (70 wt %), carbon black (Denka, 15 wt %) as a conductor, and polyvinylidene fluoride (PVDF) dissolved in *N*-methyl pyrrolidinone (NMP) as a binder (15 wt %) on copper foil substrates after which they were pressed and dried at 120 °C for 4 h under a vacuum. Laboratory-made, coin-type, electrochemical cells were assembled in an Ar-filled glovebox using Celgard 2400 as a separator, Li foil as the counter and reference electrodes, and 1 M $LiPF_6$ in ethylene carbonate (EC)/diethyl carbonate (DEC) (1:1 by volume, Samsung) as an electrolyte. All of the cells were tested galvanostatically at various voltage windows (between 0.0 and 2.0 V and 0.55 and 2.0 V vs Li/Li^+) with a current density of 100 mA g^{-1} using a Maccor automated tester, with the exception of the rate-capability tests. Li was inserted into the electrode during discharging, and it was extracted from the working electrode during charging.

3. Results and Discussion

Figure 1a,b shows the XRD patterns of the tetragonal ZnP_2 and ZnP_2/C nanocomposite. The two samples prepared by HEMM corresponded to tetragonal ZnP_2 (JCPDS no. 72-1626). As seen on the crystalline structure of Figure 1c, the P atoms of the tetragonal ZnP_2 sample formed singly bonded infinite spiral chains, while the Zn atoms formed spirals approximately coaxial with the P chains.[31]

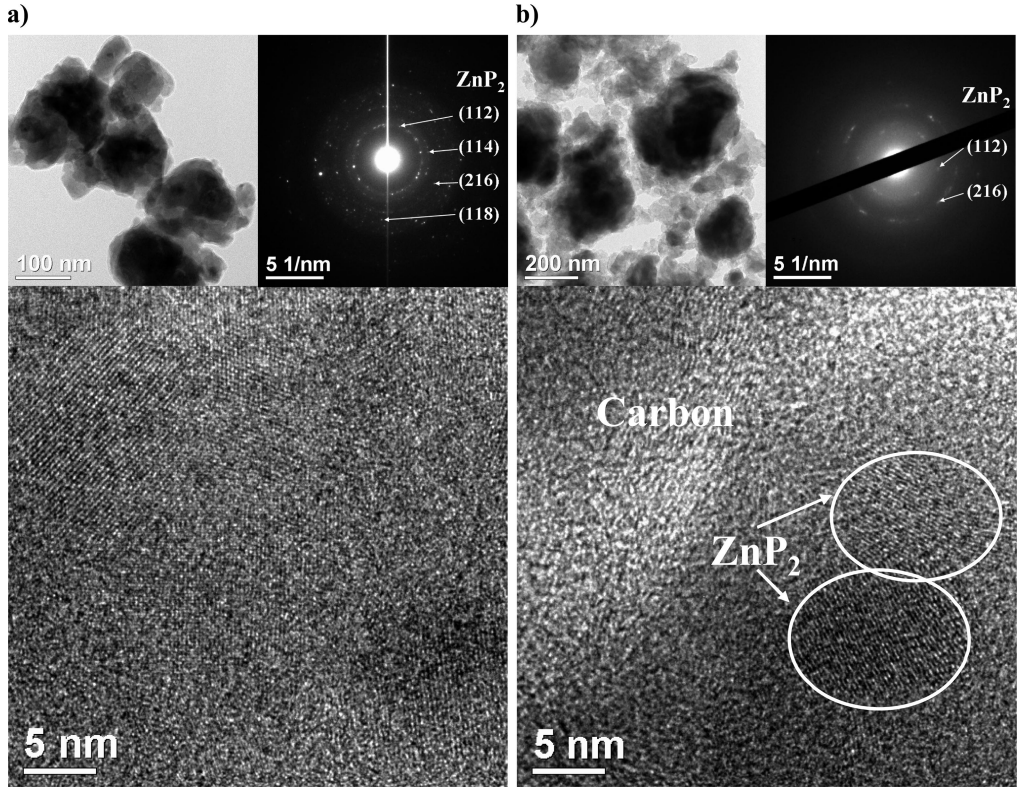

Figure 2. TEM and HRTEM images with the corresponding lattice spacing: (a) ZnP_2 and (b) ZnP_2/C nanocomposite.

TEM bright-field and high-resolution images combined with selected-area electron diffraction (SAED) pattern revealed the well developed, crystalline ZnP_2 nanoparticles (Figure 2a). Figure 2b shows the TEM bright-field and HRTEM image combined with SAED of the ZnP_2/C nanocomposite composed of approximately 200−300-nm-sized ZnP_2/C particles. Each ZnP_2/C nanocomposite particle was comprised of about 10-nm-sized ZnP_2 crystallites that were uniformly dispersed in the amorphous carbon matrix.

Figure 3a,b shows the voltage profiles of the ZnP_2 and ZnP_2/C nanocomposite, respectively. The discharge and charge capacities of ZnP_2 were 1581 mA h g^{-1} and 994 mA h g^{-1}, respectively, and it exhibited poor electrochemical reversibility. Despite its high discharge capacity, ZnP_2 had a first cycle Coulombic efficiency of only 63%. The electrochemical behaviors of the ZnP_2/C nanocomposite during the discharge/charge reaction with Li were superior to those of the pure ZnP_2 electrode, as shown in Figure 3b. The first discharge and charge capacities were 1340 mA h g^{-1} and 1107 mA h g^{-1}, respectively, and the first cycle Coulombic efficiency was about 83%. The high initial Coulombic efficiency of the ZnP_2/C nanocomposite shows that the electrochemical reaction between ZnP_2 and Li is almost reversible, given the irreversible capacity of the milled amorphous carbon (Super P) which is present (30 wt %). Preliminary study showed that the milled amorphous carbon showed a large discharge capacity of approximately 400 mA h g^{-1} while charge capacity was approximately 350 mA h g^{-1} between 0.55 and 2 V, respectively. And this indicates that the contribution to the charge capacity during the first cycle would be approximately 100 mA h g^{-1}. These enhanced electrochemical properties of the ZnP_2/C nano-

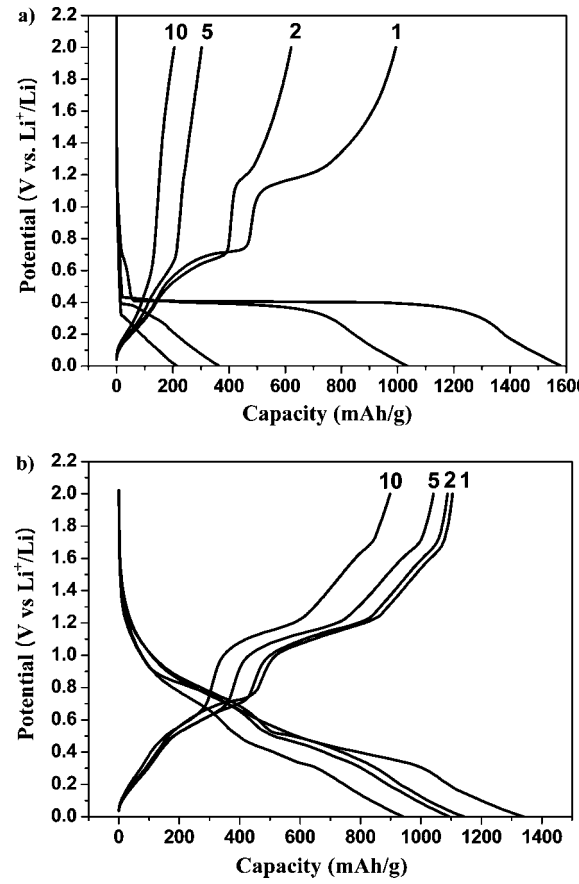

Figure 3. Electrochemical behaviors of ZnP_2 and ZnP_2/C nanocomposite: (a) voltage profile of ZnP_2 for the 1st, 2nd, 5th, and 10th cycle and (b) voltage profile of ZnP_2/C nanocomposite for the 1st, 2nd, 5th, and 10th cycle.

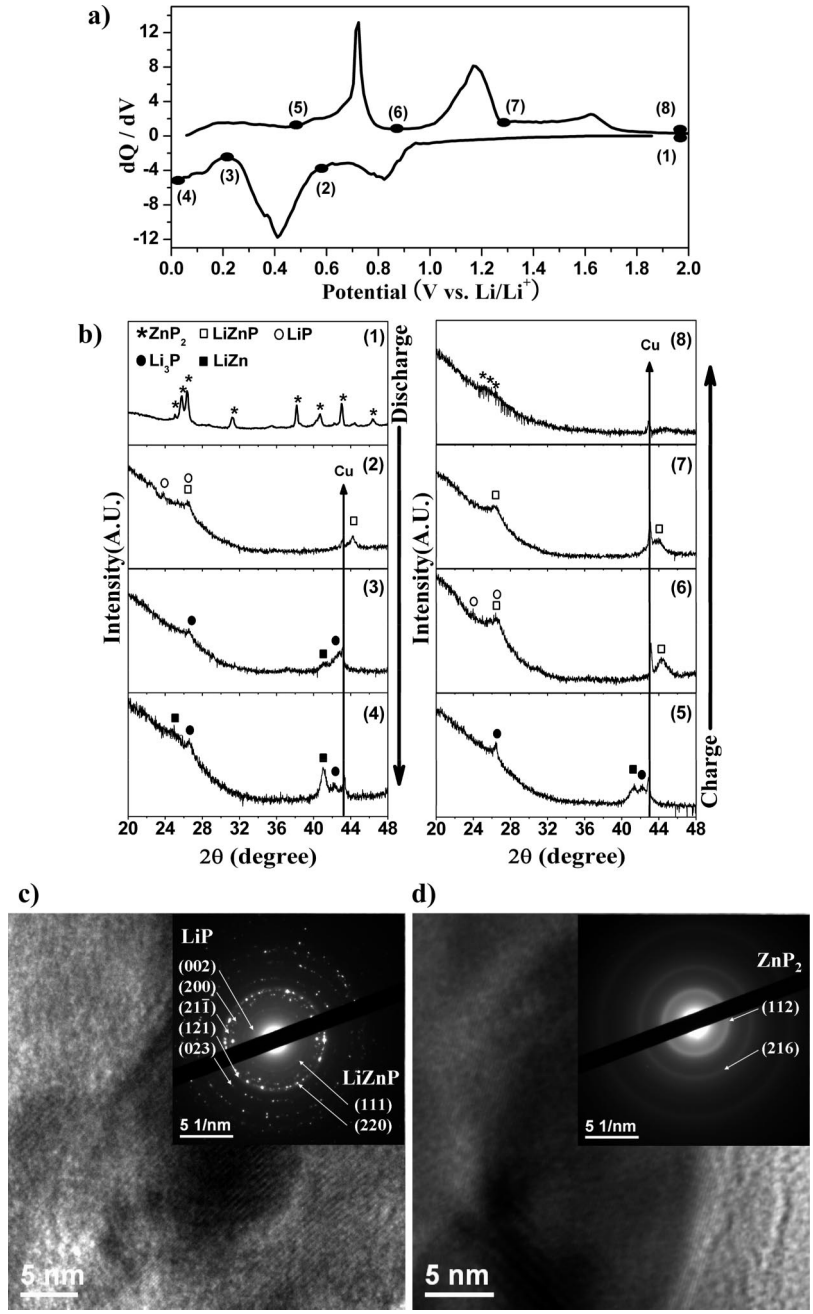

Figure 4. Electrochemical behaviors of the ZnP_2/C nanocomposite for the first cycle: (a) differential capacity plot, (b) ex situ XRD patterns of ZnP_2/C nanocomposite (numbers correspond to the voltage point indicated in Figure 4a), (c) HRTEM image with the corresponding lattice spacing of LiP and LiZnP phase formed at 0.55 V during the first discharge, and (d) HRTEM image with the corresponding lattice spacing of ZnP_2 phase formed at 2 V during the first charge.

composite contributed to its ability to provide a higher interfacial area, increase the lithium ion diffusion rate, and accommodate the strain generated during cycling by preparing uniformly distributed, nanosized, ZnP_2 crystallites in the carbon matrix.

The differential capacity plot (DCP, Figure 4a) shows three and four peaks during discharging and charging, respectively. Ex situ XRD analyses were performed at selected potentials as indicated in the DCP, and the results are presented in Figure 4b. When the potential was lowered from 2 to 0.55 V, the ZnP_2 phase disappeared and both LiZnP (JCPDS no. 42-1130) and LiP (JCPDS no. 42-0790) phases were present simultaneously, as shown in Figure 4b-(2). Ex situ HRTEM analyses were also conducted for the lithiated electrode at 0.55 V during discharging, and Figure 4c shows that both LiZnP and LiP phases were formed at 0.55 V. At a potential of 0.25 V, LiZnP and LiP phases were transformed to Li_3P (JCPDS no. 74-1160), partially developed LiZn (JCPDS no. 03-0954) phases (Figure 4b-(3)). Finally, when the potential reached 0.5 V (Figure 4b-(4)), the XRD pattern confirmed the presence of well-developed LiZn and Li_3P phases. During charging, at 0.5 V, the diffraction peak intensity of the LiZn phase was reduced, whereas that of the Li_3P peaks was unchanged (Figure 4b-(5)). At a potential of 0.9 V (Figure

4b-(6)), no Li_3P phase was observed, while the LiZnP and LiP phases reappeared. When the potential reached 1.3 V (Figure 4b-(7)), the LiP peak disappeared and only the LiZnP peaks remained. In the fully charged state (2.0 V, Figure 4b-(8)), characteristic peaks corresponding to ZnP_2 were not clear. The ex situ HRTEM analysis at a potential of 2.0 V after complete charge is shown in Figure 4d. The high-resolution image combined with SAED revealed extremely small crystallites of the ZnP_2 phase due to reconstruction reaction during charge. When fully charged, the ZnP_2 phase was reconstructed despite being completely dissociated into Li_3P and LiZn phases when fully discharged. This phenomenon is similar to that observed with Cu_6Sn_5[36] and SnSb,[37] which is also supported by the same charge and discharge behaviors of voltage profiles at various cycles in Figure 3b.

These results presented above suggest that the following reactions are involved during the first discharge and charge cycle.

During the first discharge is

$$ZnP_2 \rightarrow LiZnP + LiP \rightarrow Li_3P + LiZn$$

During the first charge is

$$Li_3P + LiZn \rightarrow LiZnP + LiP \rightarrow LiZnP\ (+\ P) \rightarrow ZnP_2$$

During the course of reactions, intermediate phases, such as Li_xP (LiP_7, LiP_5, and Li_3P_7)[38] or $LiZn_y$ ($LiZn_4$),[27] can be formed, although these phases were not identified.

The cycle performances were compared for the ZnP_2 (voltage range: 0.0−2.0 V) and ZnP_2/C nanocomposite (voltage range: 0.0−2.0 V and 0.55−2.0 V) electrodes. As shown in Figure 5, the ZnP_2 electrode exhibited very poor cycle performance within the voltage range between 0.0 and 2.0 V. When the ZnP_2/C nanocomposite was cycled within this voltage range, the cyclability was greatly enhanced compared with that of the ZnP_2 electrode, although the capacity faded to less than 200 mA h g^{-1} after 45 cycles due to mechanical cracking and crumbling caused by the large volume change originating from the formation of the Li_3P and LiZn phases. For the voltage range between 0.55 V (corresponding to the LiP and LiZnP phases) and 2.0 V (corresponding to the ZnP_2 phase), the test electrode showed excellent cycle performance with a relatively large capacity of about 350 mA h g^{-1} (or 1250 mA h cm^{-3}) over 100 cycles. The inset graph of Figure 5 shows the voltage profiles of the ZnP_2/C nanocomposite cycled between the same voltage range for the 1st, 25th, 50th, and 100th cycles, with the same behaviors being exhibited during the discharge and charge cycles. The first discharge and charge capacities of 515 mA h g^{-1} (ca. 1828 mA h cm^{-3}) and 406 mA h g^{-1} (ca. 1440 mA h cm^{-3}) at a current rate of 100 mA g^{-1}, respectively, were higher than those of commercially available graphite anodes (372 mA h g^{-1} or ca. 840 mA h cm^{-3}. These good electrochemical properties were attributed to relieved volume change or reduced structural modifications between the LiP, LiZnP, and ZnP_2 phases.

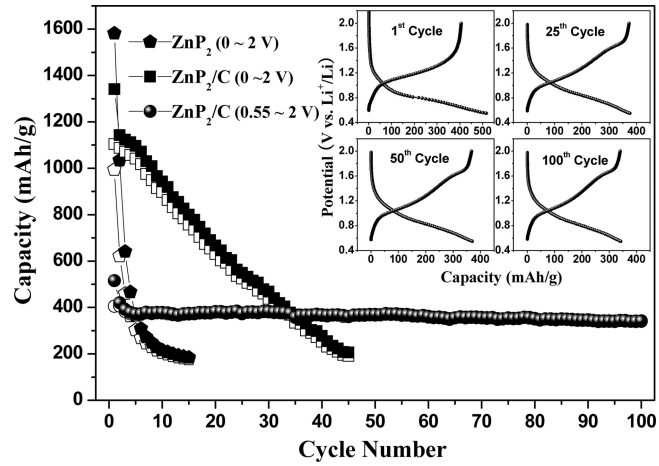

Figure 5. Comparison of cycle performances of ZnP_2 and ZnP_2/C nanocomposite at a rate of 100 mA/g. Discharge and charge capacity was shown by filled and empty patterns, respectively. (Inset graph: voltage profiles of ZnP_2/C nanocomposite cycled between 0.55 and 2 V for the 1st, 25th, 50th, and 100th cycles, respectively, showing the same behaviors during discharge and charge).

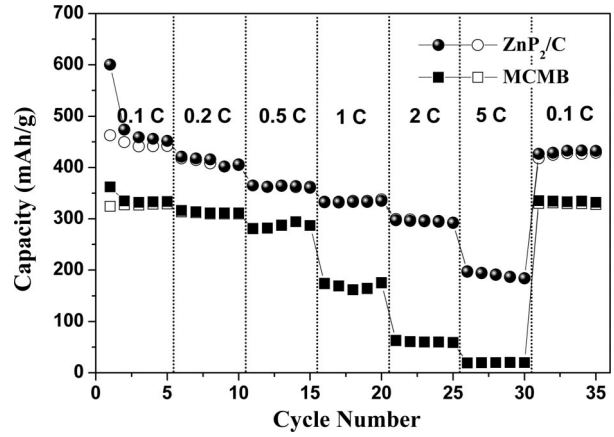

Figure 6. Plot of discharge and charge capacity vs cycle number of the ZnP_2/C nanocomposite and MCMB at various C rates (discharge capacity, filled symbols, and charge capacity, empty symbols).

The rate capability of the ZnP_2/C nanocomposite electrode was also tested. The cyclability of this electrode as a function of the C rate is shown in Figure 6, with C being defined as the full use of the charge capacity (400 mA h g^{-1}) in 1 h. This electrode exhibited a good high-rate capability and a very good charge capacity of approximately 300 mA h g^{-1} and 200 mA h g^{-1} at rates of 2 and 5 C, respectively, with stable cycling behavior. The rate-capability of the ZnP_2/C nanocomposite electrode was far better than that of the commercially used, MCMB-graphite, anode material, as compared in Figure 6.

4. Conclusion

In conclusion, tetragonal ZnP_2 particles were prepared using commercially available amorphous red phosphorus and zinc powder by HEMM without any heat treatment

(35) Davis, R. M.; McDermott, B.; Koch, C. C. *Metall. Trans.* **1988**, *A19*, 2867.
(36) Kepler, K. D.; Vaughey, J. T.; Thackeray, M. M. *Electrochem. Solid State Lett.* **1999**, *2*, 307.
(37) Francisco, J.; Fernández-Madrigal, F. J.; Lavela, P.; Vicente, C. P.; Tirado, J. L.; Jumas, J. C.; Olivier-Fourcade, J. *Chem. Mater.* **2002**, *14*, 2962.
(38) (a) JCPDS, file no. 73-1162. (b) JCPDS, file no. 73-1161. (c) JCPDS, file no. 77-2425.

or chemical methods. Further modification with amorphous carbon to form the ZnP_2/C nanocomposite produced an anode material for Li rechargeable batteries that showed a highly reversible reaction with Li. The discharge and charge capacities were 1340 and 1107 mA h g^{-1} for the ZnP_2/C nanocomposite, respectively, and the first cycle Coulombic efficiency was about 83%. Additionally, excellent cyclability with a relatively large capacity of about 350 mA h g^{-1} (or 1250 mA h cm^{-3}) over 100 cycles and a high rate capability was also achieved by controlling the voltage window. Although these superior electrochemical properties demonstrated by the ZnP_2/C nanocomposite electrode confirm its potential as a new alternative anode material for Li-ion batteries, active lithium phosphides would react with moisture in air to release toxic gas if the fully charged cell is broken, and further protective devices are needed for commercial use.

Acknowledgment. This work was supported by the Korea Science and Engineering Foundation (KOSEF) through the Research Center for Energy Conversion and Storage at Seoul National University (Grant R11-2002-102-02001-0).

CM800632F